Engineering Geology 340 (2024) 107668

Contents lists available at ScienceDirect

Engineering Geology

journal homepage: www.elsevier.com/locate/enggeo

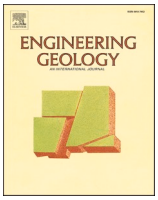

Scale and suction effects on compressibility and time-dependent deformation of mine waste rock material

Rodrigo Osses [a,b], Jubert Pineda [c], Carlos Ovalle [d,e,*], Sandra Linero [c,d,e,f], Esteban Sáez [b]

[a] Facultad de Ingeniería y Ciencias, Universidad de La Frontera, Chile
[b] Dept. of Structural and Geotechnical Engineering, Pontificia Universidad Católica de Chile, Chile
[c] University of Newcastle, Faculty of Engineering and Build Environment, Australia
[d] Dep. of Civil, Geological and Mining Engineering, Polytechnique Montreal, Québec, Canada
[e] Institute for Research in Mines and the Environment (IRME) UQAT-Polytechnique, Quebec, Canada
[f] SRK Consulting (Australasia), Australia

ARTICLE INFO

Keywords:
Creep
Mine waste rock
Particle crushing
Size effect
Suction

ABSTRACT

Designing high mine waste rock piles for long-term behavior requires material mechanical characterization over a large range of stresses and variable environmental conditions. However, representative coarse samples cannot be handled by standard testing devices and the common approach is to test small-scaled samples at the laboratory, which might be affected by particle size effects when compared to the field material. Several reported results indicate that coarser samples present higher amount of particle crushing than small-scaled samples, thus lower dilatancy and higher compressibility. However, specific studies of size effects on time-dependent deformation are lacking. The aim of this paper is to identify the effects of particle size and suction on stress-deformation mechanism of partially saturated mine waste rock. Oedometric compression tests on two parallel graded samples are presented: the gravelly fraction (d_{max}=50 mm) and the sandy fraction (d_{max}=2.36 mm). Each stress increment triggers « instantaneous » and delayed strains. The results reveal the combined effects of particle size and humidity on the mechanical behavior. Coarser samples exhibit higher total compressibility and creep deformation, which also increases with the material humidity. The results give empirical support for the development of scaling laws and suggest that total deformation can be decoupled considering a suction dependent index for creep deformation.

1. Introduction

Substantial volume of waste rock (WR) must be removed to retrieve ore in deep open pit mines. Blasted WR results in coarse angular granular material with varied grading depending on the rock damage and extraction method. The enormous growth of the mining industry in recent years has led to a significant increase in waste rock produced annually. Commonly, WR material is stored in piles that can easily reach several hundred meters high (Valenzuela et al., 2008; Zapico et al., 2020). To reduce environmental impacts and avoid instability issues, mine WR piles must be designed to ensure chemical, hydrogeological and mechanical stability (Aubertin et al., 2002; Hawley and Cunning, 2017). For the latter, the shear strength is typically evaluated through relatively large shearing tests (Ulusay et al., 1995; Linero et al., 2007, 2020; Bard et al., 2012; Ovalle et al., 2023) and stability analyses are performed using advanced numerical approaches (Steiakakis et al., 2009; Bao et al., 2019; Hoy et al., 2024).

Provided that a WR pile is mechanically stable, deformations are rarely considered as part of the design criteria. However, specific engineering designs aiming to ensure a safe mine closure plan could necessitate the estimation of settlements in the long term. This is particularly the case of open pit backfilling, which represents a prominent alternative to control the environmental impacts, reduce the altered natural surfaces by waste storage facilities and minimize landscape reshaping. For instance, mining regulations for iron mining in the Pilbara region of Western Australia require pits to be backfilled under certain conditions such as water quality (Green, 2009). According to the design criteria, a pit can be backfilled above the water table, or a pit lake can be formed (Bozan et al., 2022). In the first case, settlements should be controlled to avoid altering the surface drainage conditions or the hydraulic design of

* Corresponding author.
E-mail address: carlos.ovalle@polymtl.ca (C. Ovalle).

https://doi.org/10.1016/j.enggeo.2024.107668
Received 5 April 2024; Received in revised form 27 June 2024; Accepted 30 July 2024
Available online 2 August 2024

the closure plan. Therefore, while volumetric strains of crushed rocks can easily reach 10% at vertical pressure of about 2 MPa (corresponding to approximately 100 m of WR fill) (Oldecop and Alonso, 2003; Ovalle, 2018; Osses et al., 2021), a deep pit can lead to settlements of >10 m, eventually being incompatible with the closure plan. Moreover, since the design should be planned for the long term, creep behavior should also be considered in settlement assessments.

Motivated by large projects involving WR piles and rockfill dams, the mechanical behavior of coarse blasted and crushed rocks have been largely studied in the past (Marsal, 1967; Marachi et al., 1969; Barton and Kjaernsli, 1981; Indraratna et al., 1993; Varadarajan et al., 2003; Linero et al., 2007; Bard et al., 2012; Ovalle et al., 2020). The main challenge is that these materials cannot be handled in laboratory samples for mechanical testing, because oversized particles can easily approach 1000 mm in size, while the largest shearing devices ever built can test samples of maximum particle size (d_{max}) up to 100 to 200 mm (Leussink, 1960; Marsal, 1967; Marachi et al., 1969; Verdugo and De la Hoz, 2006; Hu et al., 2011). Therefore, small-scaled samples using the scalping or the parallel grading techniques are usually prepared to carry-out shearing or compression tests, which could be affected by size effects compared to the coarser material in the field.

Particle size effects can be examined by preparing samples at different scales at the laboratory, in order to propose scaling laws and thus extrapolate the results to the field scale (Frossard et al., 2012; Yin et al., 2017). Empirical evidence shows that, under a given loading path, the amount of particle crushing increases with the characteristic grain size, thus decreasing dilatancy and peak shear strength and increasing compressibility (Marachi et al., 1969; Alonso et al., 2005; Ovalle et al., 2014). This is mainly due to higher probability of finding weak microcracks in coarse rock aggregates, hence decreasing their crushing strength with particle size. According to the Stress Corrosion Cracking (SCC) mechanism (Scholz, 1968; Atkinson, 1984), microcrack growth within solid grains evolves upon loading and could get affected by corrosive agents (e.g. humidity), resulting in time-delayed particle crushing. A number of authors have stated that these late events of crushing are responsible for creep deformation in granular assemblies (Lade and Karimpour, 2010; Brzesowsky et al., 2014; Zhang and Buscarnera, 2017; Ovalle, 2018; Sohn and Buscarnera, 2019; Andò et al., 2019; Ovalle and Hicher, 2020). While the effects of particle size on shear strength and total deformation have been widely studied, the impact of particle size on creep deformation is still poorly understood, and recently limited studies have been reported on this topic (Xu et al., 2019; Zhou et al., 2019; Chen et al., 2021). Moreover, few works have also included the effects of humidity on creep deformation of crushable granular materials (Oldecop and Alonso, 2003; Alonso et al., 2016; Osses et al., 2021; Mao et al., 2023) and empirical evidence of the coupled effects of particle size and humidity on creep deformation are rare (Alonso et al., 2005).

The aim of this paper is to identify the combined effects of particle size and humidity (through varying total suction) on the compressibility and creep of crushable mine WR material. Saturated and partially saturated oedometric tests are presented using the parallel grading technique, in order to compare the results on two scaled samples of the same material: sandy and gravelly fractions. The effects of stress level, total suction and particle size on time-dependent deformation are analyzed and discussed.

2. Experimental framework for unsaturated coarse granular materials through total suction control

According to the SCC theory, the degree of humidity that could have a corrosive effect occurs at the tip of stressed microcracks within solid rock particles. In partially saturated crushed rock having sizes of sands and gravels, matric suction (s, defined as the difference between air pressure and water pressure) typically varies around 10 to 100 kPa and is carried by surface tension in a curved gas-liquid interface on interparticle wetted contacts (i.e. capillary bridges) (Fredlund and Rahardjo, 1993). Under this condition, one can reasonably assume that intraparticle voids and microcracks remain saturated with water, because those low values of s are not high enough to drain water from such microscopic voids. However, a significant increase in suction might be able to reduce humidity in microcracks, eventually decreasing the degree of crack corrosion. This can be achieved by drying the material up to a point where no capillary meniscus interaction lasts between grains, while a liquid phase could still exist within microcracks. This condition can be reached by controlling air humidity, imposing air advection transport through the pores, and allowing intraparticle liquid to be in equilibrium by vapor diffusion with the air of the interparticle voids (Oldecop and Alonso, 2003). For this purpose, a convenient alternative is the vapor control technique, where relative humidity (RH) of the air is in equilibrium within a closed system of constant vapor mass. Thus, total suction (ψ), which includes matric suction (s) and osmotic suction (π, related to ionic concentration of pore water), can be estimated by Kelvin's law (Fredlund and Rahardjo, 1993):

$$\psi = s + \pi = -\frac{RT}{v_{w0}\omega_v} ln(RH) \quad (1)$$

where T is temperature, R is the universal gas constant (8.31432 J/[mol K]), v_{w0} is the specific volume of water, or the inverse of the water mass density ($1/\rho_w$ m^3/kg) and ω_v is the molecular mass of the water vapor (18.016 kg/mol). According to Eq. 1, a given ψ can be targeted by controlling constant RH in a system where liquid and gas phases are at equilibrium. Control of air RH in a closed system can be assessed by allowing air to come into contact with saline solutions (Blatz et al., 2008). The method is based on the fact that water is present in both gas and liquid phases, while salt molecules can be found only in liquid. Thus, dilution of salts prevents that water molecules escape into the air and affect their concentration in the gas. By changing the chemical composition of the salt and its concentration in the liquid phase, one can vary the air RH in the system at equilibrium.

3. Mine waste rock material

The material tested was sampled from an iron mine in the Hamersley province, located in the Pilbara region of Western Australia. The Hamersley area contains the most extensive Banded Iron Formations (BIF) globally, deposited about 2400 million years ago in the late Archaen early Proterozoic era and extending over about 120,000 km^2 (Morris, 1993; Duuring et al., 2017). Mineralization is also found in channel iron deposits, which are fluvial deposits generated from unconsolidated layers rather than basement rocks, and typically covered by unmineralized BIF clasts (Kepert et al., 2010). The sampled material consists of Neogene alluvial and colluvial sediments that partly cover channel iron deposits. These sediments are typically originated from weathering, erosion and transportation of BIF rocks. As shown in Fig. 1, the samples involve alternate beds and laminae of haematite or magnetite and chert in the range of 1 mm. The specific gravity of solids (G_s) is correlated with particle size, fine particles being denser than coarse ones: $G_s = 3.87$ for grains finer than 4,75 mm, while coarser grains have $G_s = 3.32$. An X-ray Diffraction (XRD) test was performed in a D2 Phaser Bruker AXS powder diffractometry at 30 kV and 10 mA, using Cu—K (alpha) radiation. Fig. 2 presents the XRD analysis using the X'Pert HighScore Plus software, which indicated that predominant phases are silica in the form of Quartz and Haematite.

Linero et al. (2017) analyzed the shapes of Pilbara WR particles using three descriptors: elongation I/L, flatness S/I and roundness R_r; where L, I and S are the largest, the intermediate and the shortest dimensions of individual particles along three perpendicular axes, and R_r is defined according to Wadell (1932) as the relative sharpness of particle corners. All particles in between 1 and 50 mm in size have similar elongation of $0.8 < I/L < 1$ and classify as sub-rounded with $0.25 < Rr < 0.5$. Linero

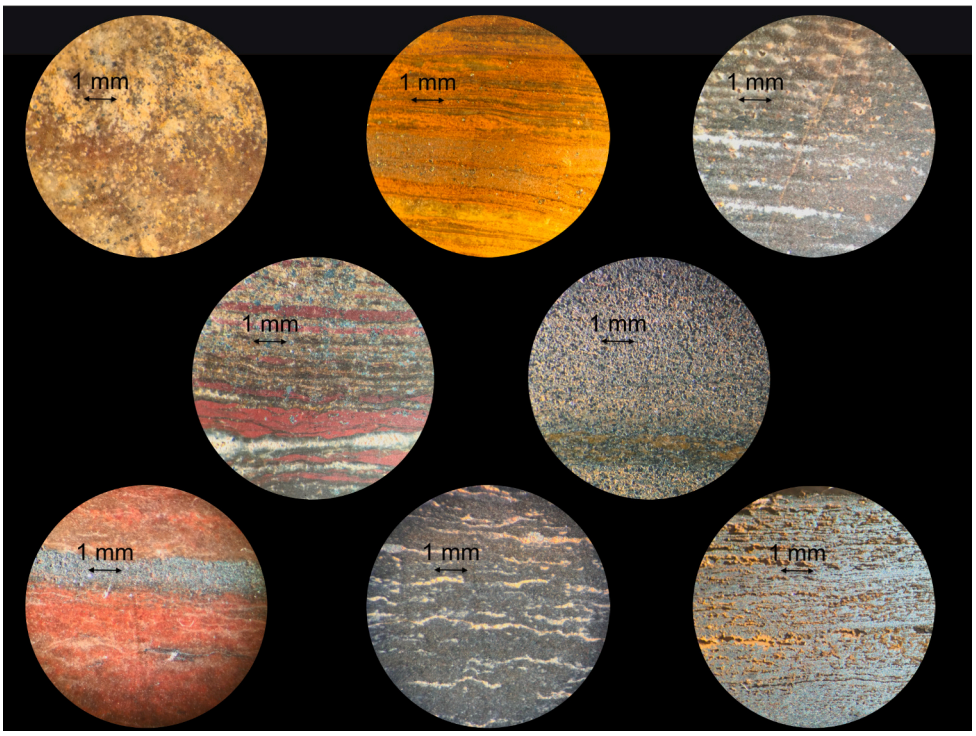

Fig. 1. Pictures of polished fragments (grey grains are haematite and magnetite, red and orange material is chert). (For interpretation of the references to colour in this figure legend, the reader is referred to the web version of this article.)

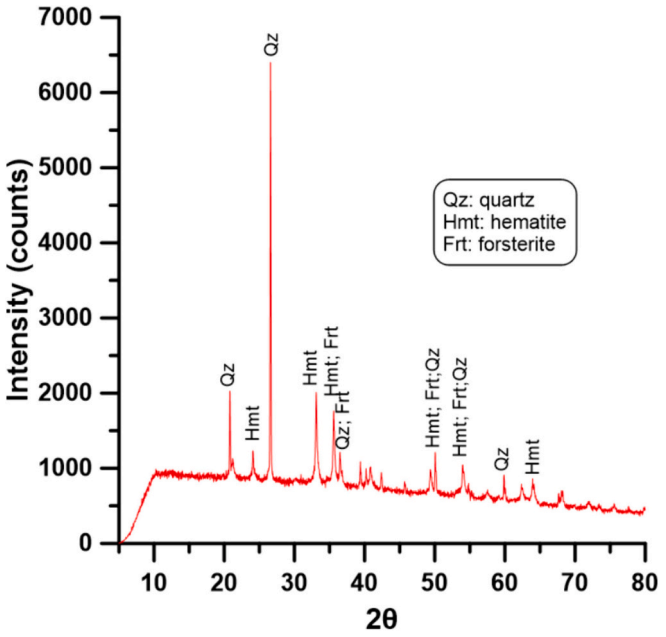

Fig. 2. XRD analysis of crushed Pilbara waste rock material.

et al. (2017) indicated that larger particles tend to be more platy or discoidal (i.e. less elongated and flatter) than smaller particles. The laminated fabric of the natural rock, which explains the variability in flatness ratio with particle size, promotes particle breakage following the lamination, i.e. perpendicular to their thickness (dimension S).

As shown in Fig. 3, two samples were selected from the material, corresponding to gravelly G and sandy S fractions, having parallel particle size distributions (psd) and coefficient of uniformity $C_u = 2$. According to the ASTM D2487-17, 2020 standard, the coarser G material, with d_{max}=50 mm and minimum particle size d_{min}=9.5 mm, classifies as gravel, while the finer material classifies as sand, having d_{max}=2.36 mm and d_{min}=0.3 mm. Both samples contain particles classifying as flat blocks, and mean values of flatness ratio S/I slightly vary from 0.55 for sandy fraction to 0.45 for the gravelly fraction. Hence, it can be assumed that the shapes of the grains are similar along the range of particle sizes contained in sandy and gravelly fractions.

Fig. 4 shows the water retention curve (WRC) of the sandy fraction ($0.3 < d < 2.36$ mm), defined in terms of gravimetric water content versus total suction. Samples were prepared using 3 layers of 40 mm in diameter and 5 mm in height. Compaction of each layer to an average void ratio of $e = 0.897$ was achieved by vibration under constant vertical stress given by a 2 kg. The WRC was obtained by exposing samples to controlled wetting and drying paths using the vapor transfer technique (Blatz et al., 2008). After achieving moisture equilibrium with the surrounding vapor phase (relative humidity or total suction), each sample was placed inside a dew-point psychrometer (WP4C: Decagon Devices®, 2018) to measure total suction); more details of the experimental procedure can be found in Osses et al. (2021). Experimental results in Fig. 4 were fitted with the van Genuchten model proposed by Jacinto et al. (2009):

$$\omega = \omega_{sat}\left[1 + \left(\frac{\psi}{P_0}\right)^{\frac{1}{1-\alpha}}\right]^{-\alpha} \quad (2)$$

where ω_{sat} is the gravimetric water content at saturated conditions, and P_0 and α are fitting parameters shown in Fig. 4 for wetting and drying paths. A value of $\omega_{sat} = 2.9\%$ was fitted and ω of the rock particles for total suction of 340 MPa is around 0.5%. Note that these values are given for $\psi > 0.2$ MPa and correspond to water storage capacity of crushed rock materials within intraparticle voids. The results are in a similar range compared to slate crushed rock particles tested by Oldecop and Alonso (2003) and andesite rock particles reported by Osses et al. (2021).

It is worth noting that the range of total suction applied in the tests (from 0 to 340 MPa) covers a broad spectrum of field conditions. For

(a)

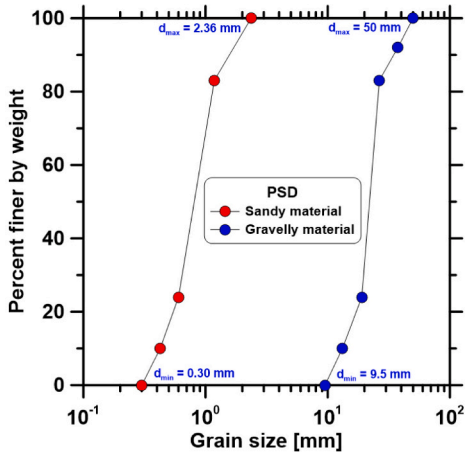

(b)

Fig. 3. Waste rock materials tested: (a) photo of typical rock particles separated by size fraction and (b) particle size distributions of S and G materials.

instance, environmental data in very dry areas, such as the Mojave Desert in the United States of America, the Atacama Desert in northern Chile, the Sahara Desert in Africa or the Pilbara region in Western Australia, can reach air RH as low as 10%, which corresponds to total suction values of >300 MPa at temperatures above 20 °C. Humid and rainy areas, such as tropical regions, can easily present RH of 95%, thus ψ of around 10 MPa. Therefore, the values tested in our study attempt to cover all those diverse conditions, in order to enhance the knowledge of environmental effects on the mechanical degradation of crushable material.

4. Oedometric compression tests

4.1. Sandy fraction (S)

Small-scale oedometer tests on specimens prepared with sandy

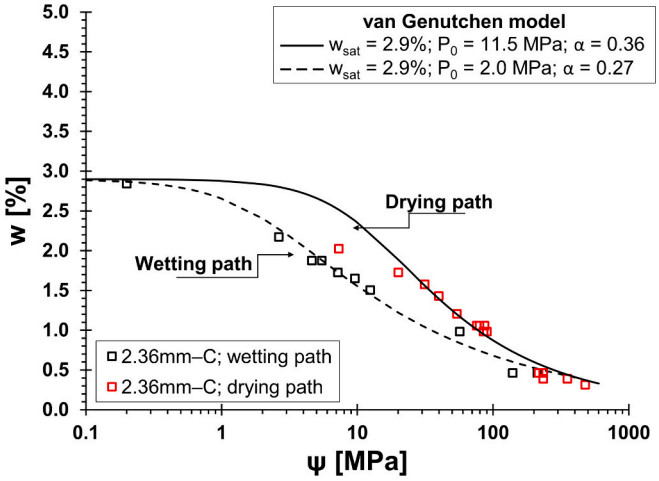

Fig. 4. Water retention curve of the sandy fraction.

fraction were performed in a cylindrical rigid cell of 48 mm in diameter and 20 mm in height, installed in a front-loading frame. Samples were prepared at $e_o = 0.897$ using the same procedure followed to obtain the WRC. Vertical stress increments were applied in steps as follows: 0.010 → 0.025 → 0.05 → 0.1 → 0.2 → 0.4 → 0.8 → 1.6 → 3.2 MPa. Each stress was maintained during 24 h aimed at assessing secondary compression behavior. For each load increment, vertical displacements were continuously recorded for 24 h (1440 min), by sampling a vertical LVDT transducer every 0.25 s through a data acquisition system.

Tests were carried-out at constant total suctions of $\psi = 0$ (fully saturated), 150, 200 and 330 MPa. Table 1 presents the summary of the tests. For $\psi = 0$ MPa, samples were flooded with deionized water 30 s after of the application of the first stress increment. On the other hand, unsaturated conditions were applied by means of the vapor transfer technique system shown in Fig. 5a (Osses et al., 2021). In this setup, the relative humidity of the air phase was controlled through a closed air-flow circuit that pass through the sample in an oedometric test. The circuit has an air pump that generates a circulating flow passing over a saline solution. Two hygrometers are used in this system for monitoring temperature and relative humidity of the air before and after passing through the tested sample. Before applying the first stress increment, 4 days of stabilization of air humidity within the air circuit were allowed. After this time, the readings of all hygrometers in the system were stable and total suction was estimated using the psychrometric law (Eq. 1). Fig. 8 shows that the air RH monitored in test S/330 was stable during the whole testing period. Table 1 presents the saline solution used in each unsaturated sample, as well as the stabilized RH value and ψ according to Eq. 1. Specific details of the experimental setup can be found in Osses et al. (2021). Each sample was sieved after testing to analyze particle breakage through changes in the psd.

4.2. Gravelly fraction (G)

Large-scale oedometer tests on gravelly fractions were performed in a large square rigid box of 720 mm × 720 mm and 600 mm in height. As shown in Fig. 6, the box and its corresponding loading frame are part of a large-scale direct shear apparatus (LDSA) developed at the University of Newcastle in Australia (Linero et al., 2020). For the tests performed in this study, the device was used only for vertical compression of samples having 235 mm in height and placed in the upper half of the LDSA box. Hence, the lateral jacks required for direct shear testing were simply not activated. The system has three 929 kN load capacity vertical jacks that apply three point loads over a 80 mm thick square steel plate placed on top of the tested sample, and two large LVDT vertical displacement transducers with a measurement range of up to 30 mm. Vertical loads

Table 1
Summary of tests on S and G samples.

Material	G_s	Test ID	Saline solution	Average RH (%)	ψ (MPa)	Max. σ_v (MPa)	Dry density (g/cm^3)	Initial void ratio, e
		S/0–1	–	–	0 (sat.)	3.2	1.984	0.925
		S/0–2	–	–	0 (sat.)	1.6	2.081	0.836
Sandy fraction, S	3.82	S/150	dry NaCl	30	150	3.2	1.984	0.925
		S/200	dry SiO_2	26	200	3.2	1.984	0.925
		S/330	dry KOH	9	330	1.6	2.039	0.873
		G/0–1	–	–	0 (sat.)	3.2	1.742	0.906
		G/0–2	–	–	0 (sat.)	3.2	1.702	0.951
Gravelly fraction, G	3.32	G/30	Saturated NaCl	85	30	3.2	1.716	0.935
		G/60	Saturated NaBr	60	60	3.2	1.682	0.973
		G/300	dry SiO_2	10	300	3.2	1.761	0.886

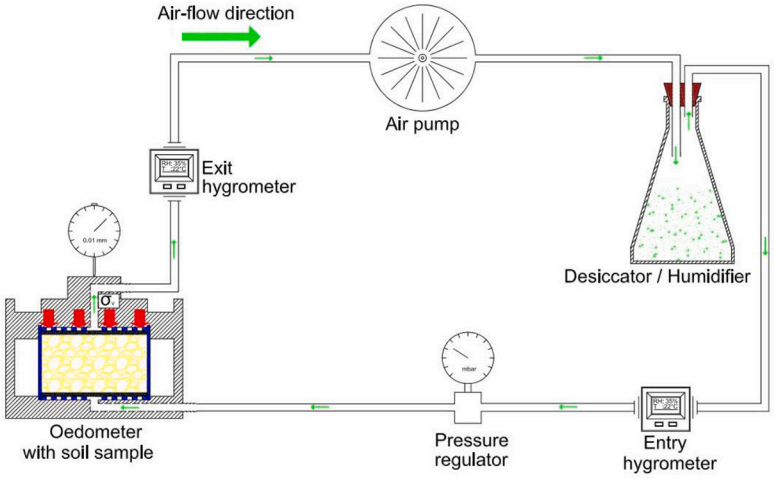

(a)

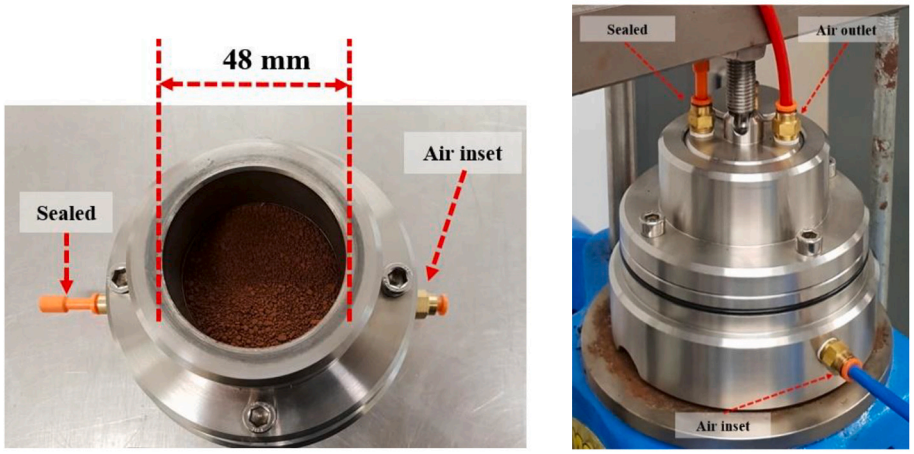

(b)

Fig. 5. Testing device for sandy material: (a) layout of the vapor control loop in oedometric tests; (b) 48 mm diameter cell for sandy Pilbara WR samples; (c) air loop for RH control.

are software-controlled in order to apply constant uniform stress on the top steel plate, so that the summation of moments of all the loads externally transmitted equals zero when calculated at the center of the sample. Vertical stress increments applied in large-scale tests were the same as for those used on sandy samples. A custom test control software was developed in the LabVIEW platform; specific details of the load control system can be found in Linero et al. (2020).

Tests on G samples were performed at constant total suctions of $\psi =$ 0 (fully saturated), 30, 60 and 300 MPa. As shown in Fig. 6a, to carry-out tests on saturated samples the large box can be housed in a watertight metallic bath containing the whole box. This bath was also used to isolate the sample and install a closed air circuit for RH control. The

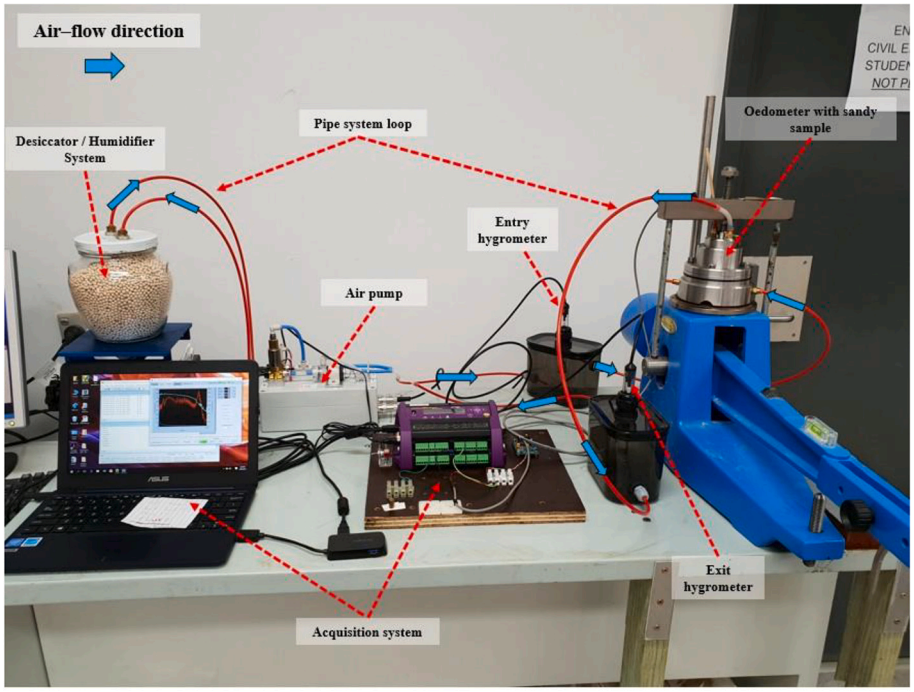

(c)

Fig. 5. (*continued*).

circuit is analogous to the one applied for sandy samples (Fig. 5), but with the additional challenges of applying it to an existing large device, which involves the implementation of greater number of air distribution piping, sealing points and monitoring instruments. To force air flow circulation through the gravelly sample, a pump was installed and controlled by software that also record temperature and RH on two hygrometers interconnected to the external piping. As illustrated in Fig. 6c, the metallic bath was sealed with a 4-mm-thick geomembrane using high resistance rubberized tape, to maintain the air system closed. Two openings have been left for air inlet and outlet. The installation and removal of the geomembrane was carried-out for each test. In order to promote a uniform distribution of the air in the sample, the single air-flow input was distributed in five pipes and located over a free space left at the inner lower half of the LDSA box (Fig. 7a), allowed by four arranged double T steel beams (Fig. 7b). In addition to RH monitoring in the external piping, two extra hygrometers with integrated dataloggers were installed in the sealed metallic bath: one located in the lower space left for air distribution (Fig. 7b) and another installed on the side of the upper box (Fig. 7d). The double T beams also fulfilled the function of supporting the lower base plate, on which the sample was arranged. To allow the passage of airflow from the lower box to the upper box, 15 mm thick perforated plywood battens were arranged over the perimeter of the base plate (Fig. 7d). In order to ensure RH homogenization, in each G sample the air humidity equalization process was maintained for 4 days, after which stable values were read on the 4 hygrometers of the system. Table 1 indicates the saline solution used for unsaturated samples, the stabilized RH value and ψ according to Eq. 1. Fig. 8 presents the RH recorded during the process, with stable values after the equalization period and holding for 9 days of oedometric testing on each sample.

Samples were prepared in four layers of homogeneous material and equal thickness. To minimize friction boundary effects, jelly vaseline was applied on the inner walls of the box, and a 0.2 mm thick poly-ethylene layer was placed on it. Each layer was filled by mixing in order to achieve homogeneity of the psd. A wooden tamper was used for compaction until reaching the target layer thick, corresponding to an average void ratio of $e_o = 0.930$ (see Table 1). Once the last layer was compacted, the horizontality of the surface of the specimen was checked with a spirit level and ensured by extra local compaction. Once the target compaction was reached, the upper plate was lifted and placed on the sample using an overhead crane, and the horizontality of the upper plate was reevaluated. Finally, through the software-controlled system, the vertical jacks were adjusted until generating a minimum uniform contact pressure of 0.01 MPa as the first applied load. It is worth noting that, compared to S samples, the higher average density achieved in G samples is limited by flat wall effects in the squared box. Compared to the circular small-scale oedometer, the configuration of the large-scale box does not allow an optimal particle arrangement on the boundaries of the sample. However, the compressibility curves and the analyses presented later demonstrate that the strain-stress relationships before yielding are reasonably similar. The main differences between the behavior of S and G samples appear in terms of particle breakage after yielding and time-dependent strains, which should not be significantly affected by the initial density.

5. Results and analyses

Fig. 9 presents compressibility curves for all tests on sandy and gravelly samples in terms of volumetric strain (ε_v) and vertical stress (σ_v). Labeling of each test is defined as X/Y-N, where X is S for sandy or G for gravelly material, Y is ψ in MPa and N is a correlative number only if there is more than one test per X/Y pair. Accurate testing repeatability was checked for $\psi = 0$ MPa in sandy samples for S/0–1 and S/0–2, and G/0–1 and G/0–2 for gravelly samples (see Table 1).

The first observation in Fig. 9 indicates that sandy samples are clearly less compressible than gravelly samples. Namely, volumetric deformation of saturated samples at $\sigma_v = 3.2$ MPa is 6% and 15% for S and G, respectively. According to size effects on grain crushing strength, this result is mainly related to higher amount of particle breakage in the coarser material. After testing, the amount of material finer than the initial d_{min} is about 2% in saturated S material and >13% in saturated G material. A quantitative assessment of the amount of particle breakage decreasing with total suction in G samples is given in Fig. 10b, through

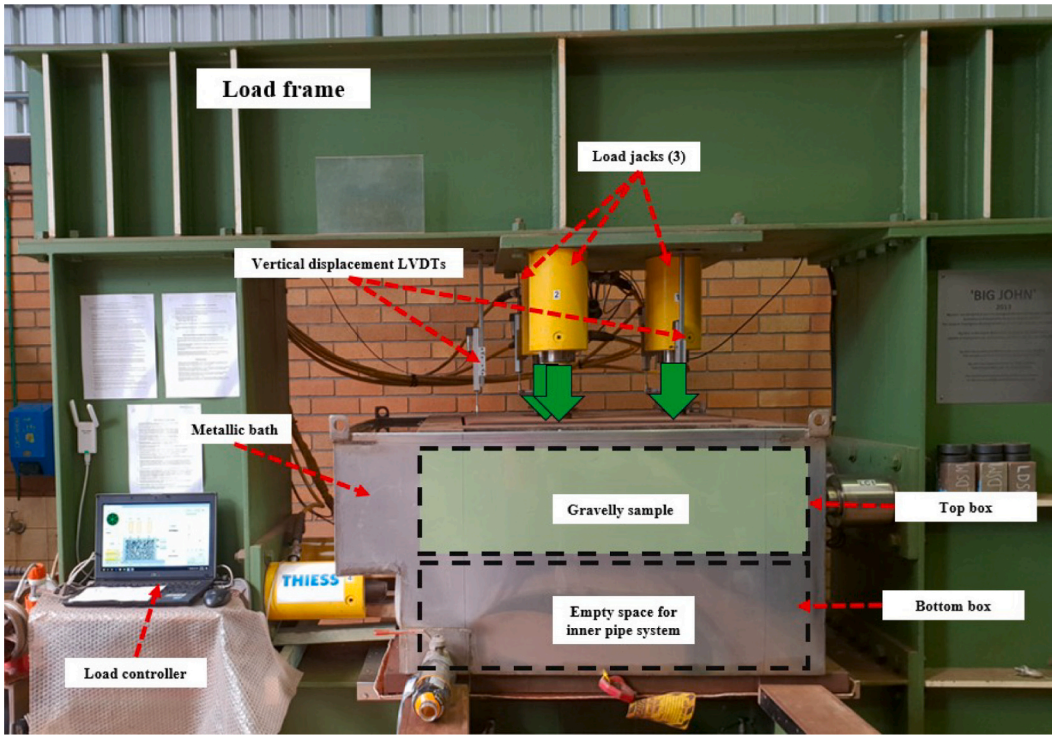

(a)

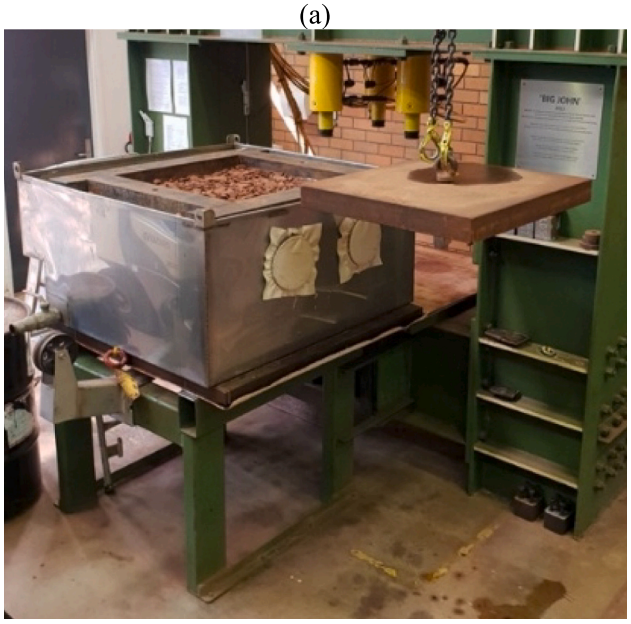

(b)

Fig. 6. Testing device for gravelly material: (a) LDSA frame and 720 mm × 720 mm box; (b) sample of gravelly Pilbara WR; (c) air loop for RH control.

the percent of the material finer than d_{min} ($d < d_{min}$= 9.5 mm) after oedometric tests at σ_v=3.2 (MPa); the value decreases from around 13% after the test at $\psi = 0$ MPa, to 9.5% at $\psi = 300$ MPa. A second observation of Fig. 9 reveals that, for a given material, compressibility increases with suction decreasing, and the largest deformation at given σ_v is always for saturated samples. For instance, at $\sigma_v = 3.2$ MPa volumetric deformation of unsaturated G samples at $\psi = 30$, 60 and 300 MPa is 11.5%, 12.0% and 12.5%, respectively, while for $\psi = 0$ MPa is between 14% to 15%. This result is expected if one assumes that SCC is the main mechanism triggering grain fragmentation.

Fig. 11 presents time-deformation curves for different constant stress during 24 h in specimens equilibrated at total suctions of $\psi = 0$, 150 and 200 MPa for sandy samples, and $\psi = 0$, 60, 300 MPa for gravelly samples. For each stress level, all cases are characterized by a sudden or « instantaneous » significant volume reduction occurring during the first seconds, followed by linear evolution of strains in logarithmic time scale until the next stress increment (i.e. during 24 h of constant stress). The latter is typically assumed to be secondary compression or creep behavior (Oldecop and Alonso, 2003; Ovalle, 2018; Osses et al., 2021). If one defines t^i as the time elapsed between the application of the stress increment and the end of instantaneous settlements (i.e. purely creep settlements take place thereafter), the secondary compression index can

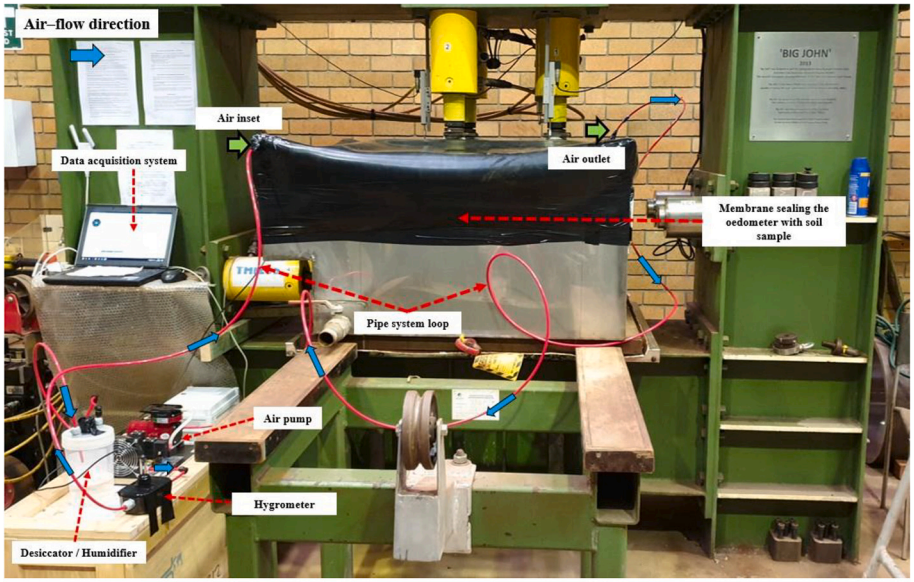

(c)

Fig. 6. (*continued*).

be obtained for $t > t^i$ as $C_\alpha = -\Delta e/[logt - logt^i]$, as conceptually illustrated in Fig. 12. According to the results in Fig. 11 and regardless of the material or testing conditions, $t^i = 1$ min has been chosen in this paper for the following analyses. This assumption agrees with reported tests in clean sands and gravels (Oldecop and Alonso, 2007; Ovalle, 2018; Sohn and Buscarnera, 2019; Osses et al., 2021), where purely creep settlements have been reported after <1 min of constant stress. On the other hand, the total strain evolution can be captured through the compressibility index $C_c = -\Delta e/\Delta log\sigma_v$ (see Fig. 12).

Fig. 13 shows the values of C_α and C_c for each stress stage on every test presented in this paper. As expected from the compressibility curves in Fig. 9, C_c of S samples are much lower than the values of G samples. At the highest vertical stress applied, C_c of S is between 0.05 and 0.15, while the values of G are around 3 to 4 times higher. Moreover, for a given material, the lower the total suction the higher the C_c. For instance, the highest C_c values obtained for G samples at $\psi = 0$, 30 and 300 MPa are 0.45, 0.36 and 0.32, respectively. Regarding creep, in all cases C_α strongly depends on ψ, which is consistent with the SCC mechanism promoting more delayed breakage degradation at higher humidity. Comparing the saturated against the driest case of G samples at $\sigma_v = 3.2$ MPa, C_α decreases from a mean value of 0.0080 after tests at $\psi = 0$ MPa, to 0.0038 at $\psi = 300$ MPa, which indicates that delayed deformation is around twice in the saturated case. Also, C_α values are around 4 times lower in S material, revealing that there is a clear particle size effect on creep strains. As far as the authors know, the latter empirical observation has been rarely reported in the literature.

Based on the empirical observation that time-dependent behavior of a given material is directly related to its total compressibility, Mesri and Godlewski (1977) proposed to characterize secondary compression behavior through the C_α/C_c ratio. The authors proposed that, regardless of the stress applied, its value can be considered as a material constant. In other words, the uniqueness of the ratio C_α/C_c applies for both the compression and recompression ranges. Mesri and Vardhanabhuti (2009) reported values of C_α/C_c= 0.01 to 0.03 for crushable sands and recently Osses et al. (2021) showed that the ratio decreases with increasing suction. Fig. 14 illustrates that C_α/C_c for all tests presented in this paper remain within the same previous reported ranges.

Hardening of crushable granular materials composed by elastic-brittle particles occurs via two main mechanisms: particle irrecoverable rearrangement and clastic yielding (McDowell and Bolton, 1998). The clastic yield stress (σ_y) is defined as the stress that triggers the onset of particle crushing. The tests on sandy fraction presented in this research showed a notably low amount of particle breakage, as confirmed by psd after testing shown in Fig. 10. A close comparison between tests S/0–1 and S/0–2 -loaded up to a maximum σ_v of 3.2 MPa and 1.6 MPa, respectively- shows that the percent of mass finer than d_{min} is of 2% and 0.5%, respectively. Assuming that this degree of breakage is negligeable for S/0–2, one can propose that the clastic yield stress of S material is $\sigma_y = 1.6$ MPa, after which a low but non-negligible amount of particle crushing can be measured. Concerning tests on the gravelly fraction, $\varepsilon_v - log\sigma_v$ plots of (a) saturated and (b) unsaturated samples illustrated in Fig. 15 indicate that clastic yield stress of G material can be set at $\sigma_y = 0.1$ MPa, where a clear shift of the compression curve is observed when compared to the compressibility of S material. According to the SCC mechanism, it is expected that σ_y should also depend on suction. However, the magnitude of the stress increments applied in this study do not allow to discriminate different yield stresses among saturated and unsaturated samples.

6. Discussion

As previously stated, assessing material size effects and creep strains in mine WR piles and open pit backfilling is of great importance to guarantee the long-term stability of closure plans. Thus, the development of predictive models is essential to advance safe designs. With the aim of further analyze and understand the results of this study on S and G materials, this section presents (a) a potential approach for size effect estimation and (b) a decoupled analysis of instantaneous and delayed strains to evidence size effect in creep strains.

6.1. Size effects

Since rock particles exhibit size effects in crushing strength, to create the same amount of particle breakage (B_r) in two scaled samples with parallel grading (such as S and G) subjected to a given stress path, a higher stress magnitude should be applied on the finer material S. Building on this evidence and applying the weakest link concept proposed by Weibull (1939), Frossard et al. (2012) developed a scaling law to estimate the shear strength envelope of G based on test results on S. This approach was later validated by Ovalle et al. (2014) using

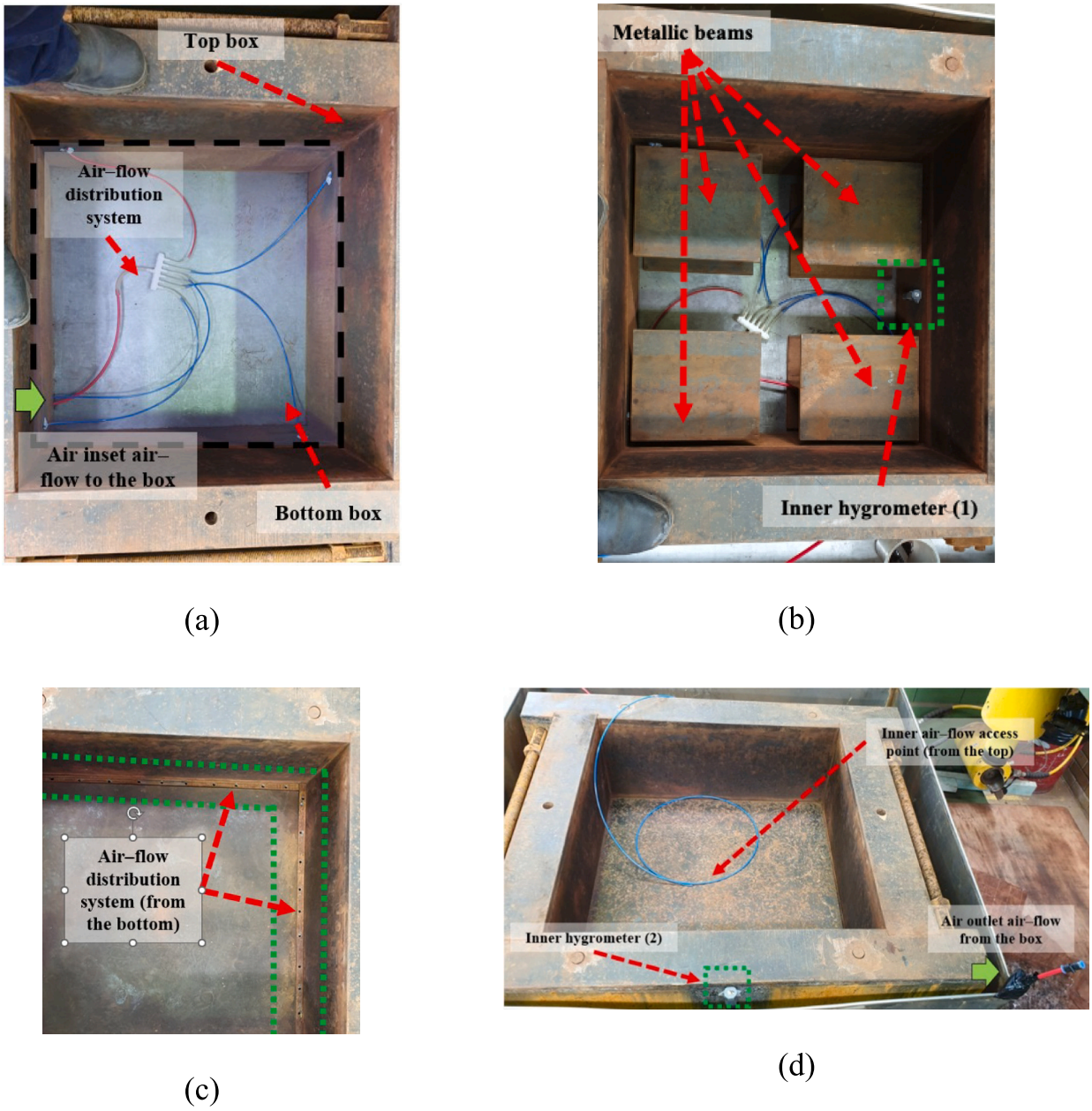

Fig. 7. Set-up at the inner bottom of the LDSA box: (a) air flow distribution, (b) beams allowing bottom free space and bottom inner hygrometer, (c) bottom system for airflow passage, (d) bottom steel plate and air flow and top inner hygrometer.

experimental data from different rockfill materials. Following the same vein, Yin et al. (2017) demonstrated that the plastic works (w^p) to reach identical B_r in S and G is given by the following relationship:

$$w_G^p(B_r) = w_S^p(B_r) \bullet \left(\frac{d_G}{d_S}\right)^{-\alpha} \tag{3}$$

where $w_S^p(B_r)$ and $w_G^p(B_r)$ are the plastic works of S and G, respectively, d_S and d_G are the characteristic particle sizes of S and G materials (e.g., d_{max}), respectively, and β is a Weibull parameter capturing size effect on particle crushing strength. Several experimental results of lump and point load tests on rock particles and sand grains have indicated β values between 0.3 and 0.5, depending mainly on rock mineralogy (Nakata et al., 1999; Lim et al., 2004; Ovalle et al., 2014). Note that, since $d_G > d_S$ and $\beta > 0$, Eq. 3 always gives $w_G^p(B_r) < w_S^p(B_r)$.

On the other hand, if the same stress path is applied on S and G, the latter will result in higher w^p due to size effect in total compressibility (i.e., in this case $w_G^p > w_S^p$). Then, hypothesizing that a relationship equivalent to Eq. 3 can be suggested to link the plastic work of S and G under such conditions, one can write

$$w_G^p(\sigma) = w_S^p(\sigma) \bullet \left(\frac{d_G}{d_S}\right)^{\beta'} \tag{4}$$

where $w_S^p(\sigma)$ and $w_G^p(\sigma)$ are the plastic work after a given stress σ, and $\beta' > 0$ is a scaling parameter reminiscent of Weibull's theory. For the sake of simplicity, one can assume $\beta' = \beta$. However, it is worth noting that size effects assessment based on Weibull's approach (Eq. 3) considers primarily clastic hardening due to particle crushing strength decreasing with size. Other mechanisms, such as particle rearrangement and friction dissipation, are not considered analytically, but could be included implicitly by calibrating β' other than β. According to these

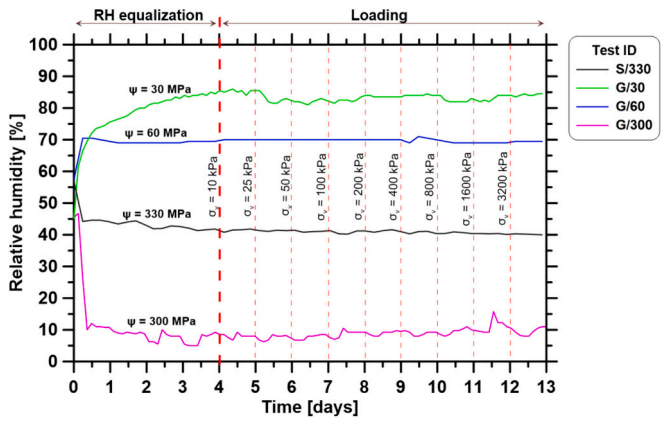

Fig. 8. Air RH records during equalization and oedometric testing on S and G samples.

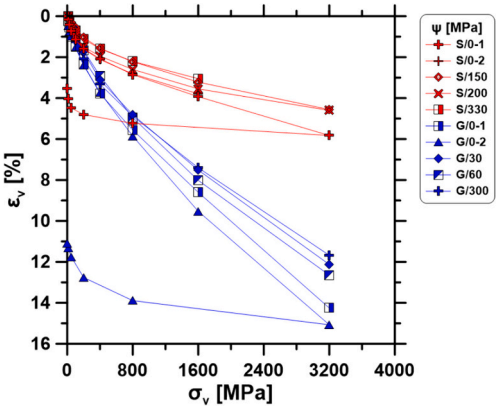

Fig. 9. Oedometric compression curves.

terms, Eq. 4 can be employed to obtain a prediction of w_G^p, as explained hereafter.

The plastic work after an oedometric test on S is given by

$$w_{S(n)}^p = \sum_j^n \sigma_{v(j)} \Delta\varepsilon_{v(j)}^p \tag{5}$$

where j is the correlative number of the stress increments (varying from $1 \rightarrow n$), $\sigma_{v(j)}$ is the cumulated stress magnitude at the j-increment, and $\Delta\varepsilon_{v(j)}^p$ is the plastic volumetric strain during the j-increment. In turn, $\Delta\varepsilon_{v(j)}^p$ is obtained as

$$\Delta\varepsilon_{v(j)}^p = \Delta\varepsilon_{v(j)} - \frac{C_s}{1+e_o}\left(log\sigma_{v(j)} - log\sigma_{v(j-1)}\right) \tag{6}$$

where $\Delta\varepsilon_{v(j)}$ is the total strain generated by the j-increment and $C_s = -\Delta e/\Delta log\sigma_v$ is the swelling index of S material, which resulted in $C_s = 0.013$ for both S/0 and S/330 tests. Using data from tests on S in Eqs. 5 and 6, setting $d_G = 50$ mm, $d_S = 2.38$ mm and $\beta' = 0.4$ (i.e., simply assuming $\beta' = \beta$, and using the mean β value reported in previous studies), Fig. 16 presents the w_G^p predictions of Eq. 4, after an oedometric loading path between $\sigma_v = 0.1 \rightarrow 3.2$ MPa. To compare tests under similar conditions, the Figure includes the cases at the lower and the highest total suctions used; namely, tests on S and G at $\psi = 0$ MPa are compared, and tests on S at $\psi = 330$ MPa are compared against tests on G at $\psi = 300$ MPa. The prediction of Eq. 4 is reasonably accurate, suggesting that this approach is suitable for scaling up compressibility to coarse materials.

Subsequently, the plastic strains on G for a given stress increment j can be obtained by differentiation of the w_G^p prediction:

$$\Delta\varepsilon_{v(j)}^p = \frac{\Delta w_{G(j)}^p}{\sigma_{v(j)}} \tag{7}$$

Finally, the prediction of the total strain of G from j to n is obtained by adding the increments $\Delta\varepsilon_{v(j)}$ given by Eq. 6. For instance, using data

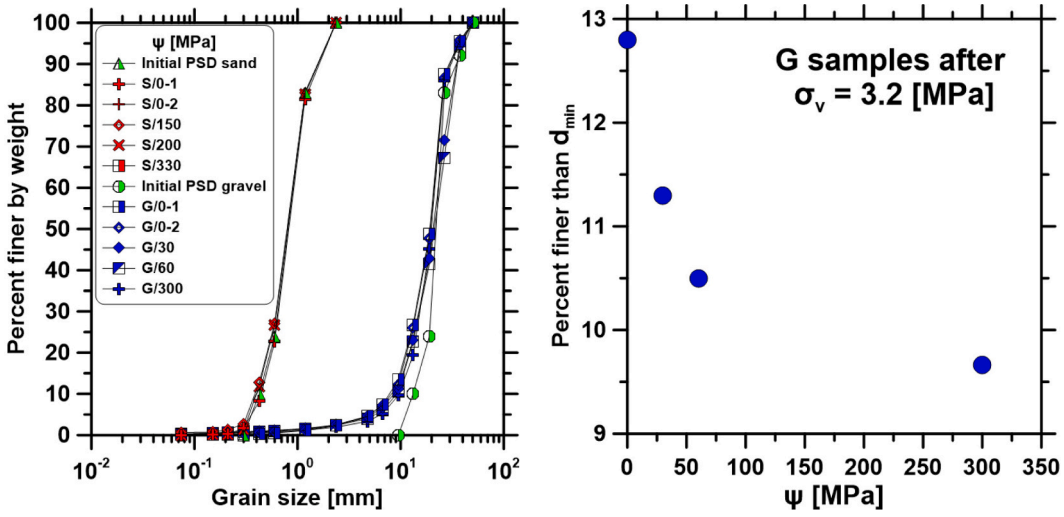

Fig. 10. Grading after testing: (a) psd after testing of all tests, and (b) percent finer than initial $d_{min} = 9.5\ (mm)$ after an oedometric test in G material at $\sigma_v = 3.2\ (MPa)$.

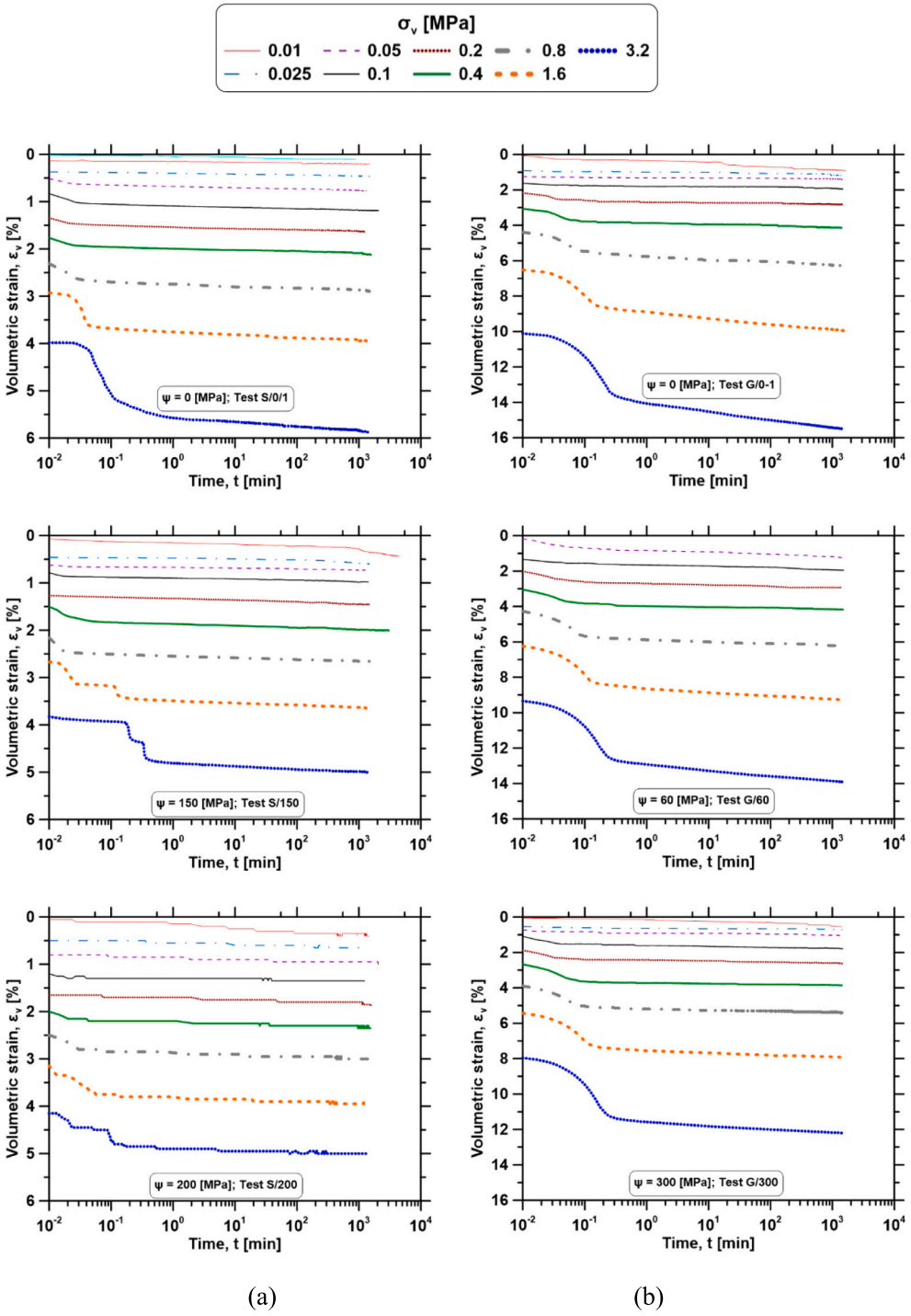

Fig. 11. Time settlement curves of (a) S samples at $\psi = 0$, 150 and 200 MPa, and (b) G samples at $\psi = 0$, 60 and 300 MPa during oedometric compression.

from the compression curve of the test S/0–1, Fig. 15a displays the prediction for G material at $\psi = 0$ MPa. Similarly, based on the test S/330, Fig. 15b presents the estimated curve for G at $\psi = 330$ MPa. Both evaluations give an accurate agreement with the experimental data for different total suctions and represent a promising approach to assess size effects. However, a validation of this method should be carried-out in future studies after comprehensive testing on several materials and, ideally, back analyses based on field monitoring of settlements under varied environmental conditions.

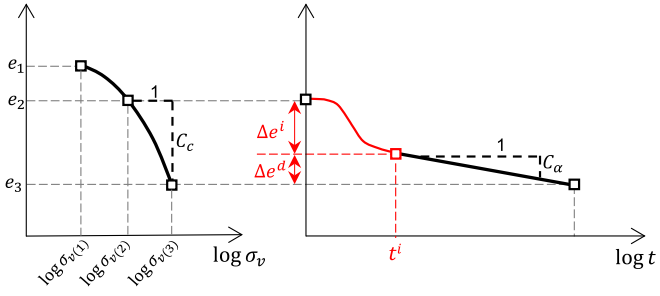

Fig. 12. Conceptual partition between initial and delayed strains.

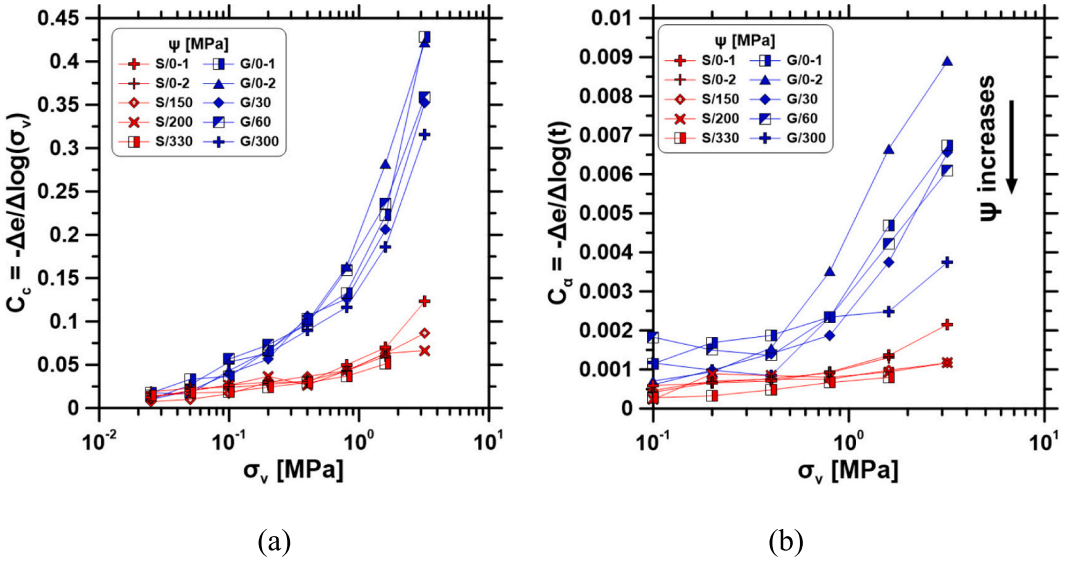

Fig. 13. (a) Compression (C_c) and (b) creep (C_α) indexes.

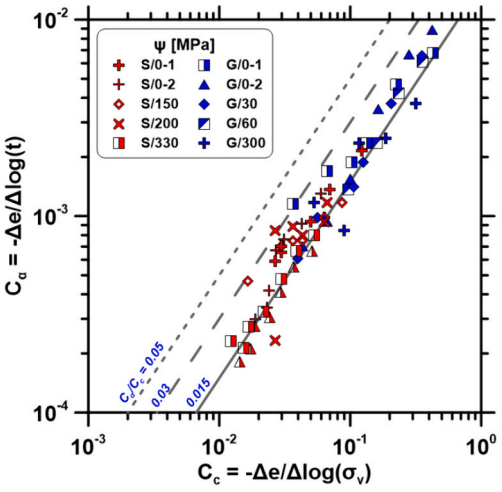

Fig. 14. Compressibility index ratio C_α/C_c of all tests at each stress increment.

6.2. Time-dependent behavior

Incremental volumetric total deformation ($\Delta\varepsilon_v$) after a given vertical stress increment under oedometric compression can be decomposed in instantaneous strains ($\Delta\varepsilon_v^i$: incremental deformation at $t^i = 1$ min) and delayed (creep) strains ($\Delta\varepsilon_v^d(t)$: incremental deformation between t^i and t):

$$\Delta\varepsilon_v(t) = \begin{cases} \Delta\varepsilon_v^i; t = t^i \\ \Delta\varepsilon_v^d(t) + \Delta\varepsilon_v^i; t > t^i \end{cases} \quad (8)$$

$\Delta\varepsilon_v^i$ includes reversible and non-reversible components, while $\Delta\varepsilon_v^d$ is related to delayed events of particle damaging and crushing, which are entirely plastic. A close observation of Fig. 11 allows to conclude that, for a given material and testing conditions, instantaneous strains are always higher than creep strains. For example, at $\sigma_v = 3.2$ MPa and $\psi = 0$ MPa, $\Delta\varepsilon_v^i \approx 1.1\%$ and $\Delta\varepsilon_v^d \approx 0.8\%$ in S samples, while $\Delta\varepsilon_v^i \approx 4\%$ and $\Delta\varepsilon_v^d \approx 1.7\%$ in G samples, which reveals a manifest scale effect. Furthermore, creep strains strongly depend on ψ, with significant increment of

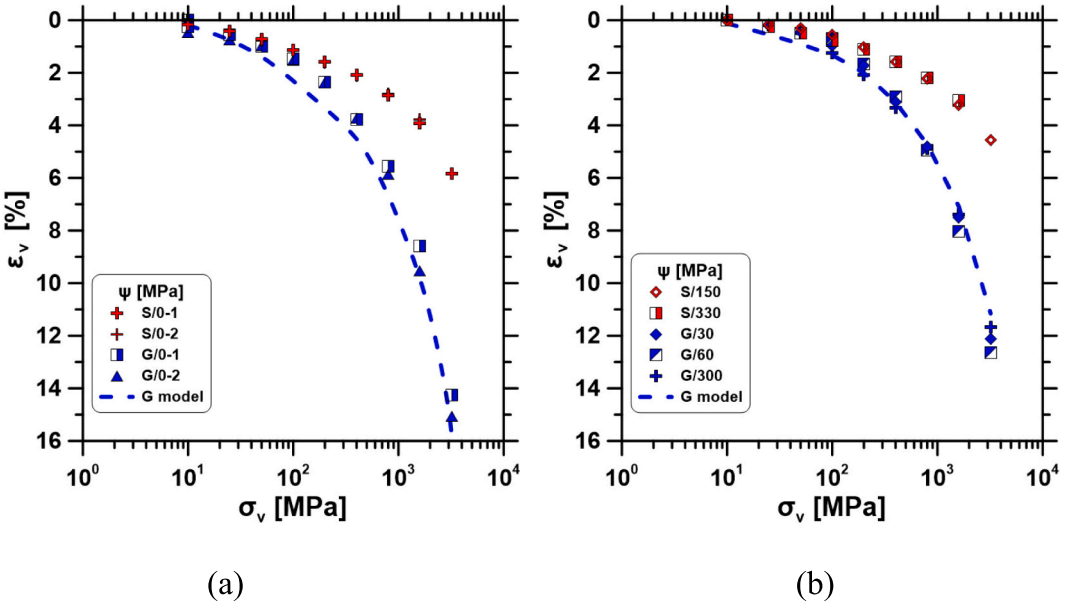

Fig. 15. Oedometric compression curves of S and G and scaling up predictions for G: (a) saturated samples and (b) unsaturated samples.

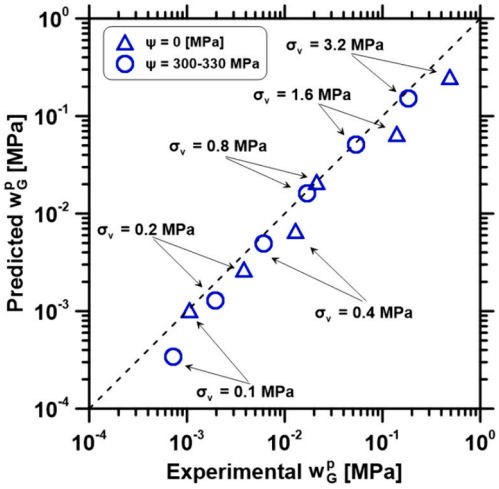

Fig. 16. Experimental vs. predicted mechanical plastic work in gravelly samples tested at total suction of 0 and 300–330 MPa, and vertical stresses from 0.1 to 3.2 MPa.

$\Delta\varepsilon_v^d$ at higher suction; e.g., in G samples $\Delta\varepsilon_d^i$ increases from 0.85% at $\psi =$ 300 MPa to a mean value of 1.7% in saturated samples. This rarely reported observation confirms that creep behavior is affected by particle size effects.

During clastic hardening (i.e., $\sigma \geq \sigma_y$), volumetric plastic strain increments ($\Delta\varepsilon_v^p$) after a vertical stress increment can be obtained by adding instantaneous ($\Delta\varepsilon_v^{p^i}$) and delayed ($\Delta\varepsilon_v^{p^d}$) plastic strains:

$$\Delta\varepsilon_v^p = \Delta\varepsilon_v^{p^i} + \Delta\varepsilon_v^{p^d} \tag{9}$$

According to the definition in Fig. 12, creep strains can be computed as

$$\Delta\varepsilon_v^{p^d} = \frac{C_\alpha}{1+e_o}\Delta log\sigma_v \tag{10}$$

Owing to acceleration of the SCC mechanism at high humidity, Fig. 13b illustrates that C_α depends on ψ. This is consistent with the model of Oldecop and Alonso (2001), who suggested a suction dependent secondary compression index. In order to verify the applicability of the previous statement, Fig. 17(a) displays C_α after tests on G samples at $\sigma_v = 1.6$ and 3.2 MPa. For a given σ_v, C_α clearly decreases with suction, which is consistent with dryer samples presenting lower corrosion effects, therefore lower creep strains.

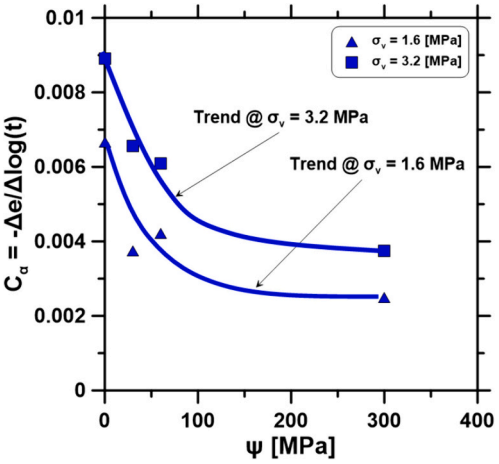

Fig. 17. Increasing C_α with total suction after tests on G material.

7. Conclusions

This paper presented experimental evidence of the effects of particle size and suction on total and time-dependent deformation of crushable granular materials. A series of oedometric compression tests on two iron mine waste rock samples, prepared from the same material but with parallel grading (sandy fraction S with $d_{max} = 2.36$ mm and gravelly fraction G with $d_{max} = 50$ mm), were carried-out under saturated and unsaturated conditions. S samples were tested in a standard oedometric cell of 48 mm in diameter, while G samples were installed and compressed in a large square box with a side of 720 mm. A closed air loop was set for each testing device, in order to control the air relative humidity within the unsaturated samples and thus calculate the total suction through Kelvin's law, obtaining values from 0 to 330 MPa. Vertical stresses applied varied from 0.01 to 3.2 MPa, and each stress increment was maintained during 24 h to measure creep deformation. The effects of the stress level, total suction and time on compressibility were analyzed and discussed. The main conclusions of this study are the following:

- For a given particle size distribution, total compressibility and creep deformation increased with decreasing suction, certainly due to degradation caused by Stress Corrosion Cracking (SCC).
- For a given suction, total compressibility was higher in G compared to S material, due to increasing grain breakage in coarser samples.
- For a given suction, creep deformation increases with particle size. This result contributes to a better understanding of the rarely reported phenomenon of size effect on time-dependent behavior of crushable granular materials.

Summarizing, the results have confirmed that the mechanical degradation of crushable granular materials is influenced by the effects of particle size and SCC mechanism. Several research works have focused separately on size effects and time-dependent behavior, however, this research offers a valuable step forward toward a better understanding of the combined mechanisms in a given material. For engineering designs, it becomes important to define the humidity range to which coarse granular fill will be subjected in the field, in order to characterize the material under such conditions. Then, if the real material has oversized clasts and small-scaled samples must be used for laboratory characterization, the results could underestimate the compressibility of the real coarser material and higher creep strains should be expected in the field. These results should be verified for different materials and extended to other stress paths, such as triaxial shearing. Afterwards, scaling laws based on Weibull's theory could be proposed. Nonetheless, given the drastic particle size reduction from potential field conditions, validation against in situ monitoring will be essential.

CRediT authorship contribution statement

Rodrigo Osses: Writing – review & editing, Methodology, Investigation, Formal analysis, Data curation, Conceptualization. **Jubert Pineda:** Writing – review & editing, Validation, Supervision, Resources, Project administration, Methodology, Investigation, Funding acquisition, Formal analysis, Data curation, Conceptualization. **Carlos Ovalle:** Writing – original draft, Supervision, Project administration, Methodology, Investigation, Funding acquisition, Formal analysis, Conceptualization. **Sandra Linero:** Writing – review & editing, Methodology, Conceptualization. **Esteban Sáez:** Writing – review & editing, Supervision.

Declaration of competing interest

The authors declare that they have no known competing financial interests or personal relationships that could have appeared to influence the work reported in this paper.

Data availability

Data will be made available on request.

Acknowledgements

This research work benefitted from the financial support of ANID Chile through project FONDECYT 11150084, the PhD Scholarship of Rodrigo Osses ("Beca Doctorado Nacional" No. 21160938) and the Natural Sciences and Engineering Research Council of Canada (NSERC) [funding reference number RGPIN-2019-06118]. Fortescue Metals Group Ltd. provided the material and supported Dr. Osses and Dr. Linero during different stages of this research; this support is greatly appreciated.

References

Alonso, E., Olivella, S., Pinyol, N., 2005. A review of Beliche Dam. Géotechnique 55 (4), 267–285.
Alonso, E., Romero, E., Ortega, E., 2016. Yielding of rockfill in relative humidity-controlled triaxial experiments. Acta Geotech. 11 (3), 455–477.
Andò, E., Dijkstra, J., Roubin, E., Dano, C., Boller, E., 2019. A peek into the origin of creep in sand. Granul. Matter 21 (11), 1–8.
ASTM D2487-17, 2020. Standard Practice for Classification of Soils for Engineering Purposes (Unified Soil Classification System). ASTM International, West Conshohocken.
Atkinson, B.K., 1984. Subcritical crack growth in geological materials. J. Geophys. Res. 89 (B6), 4077–4114.
Aubertin, M., Bussière, B., Bernier, B., 2002. Environnement et gestion des rejets miniers. In: Presses internationales Polytechnique. ISBN 9782553010309.
Bao, Y., Han, X., Chen, J., Zhang, W., Zhan, J., Sun, X., Chen, M., 2019. Numerical assessment of failure potential of a large mine waste dump in Panzhihua City, China. Eng. Geol. 253, 171–183.
Bard, E., Anabalon, M., Campaña, J., 2012. Waste rock behavior at high pressures: dimensioning high waste rock dumps. In: Hicher, P.-Y. (Ed.), Multiscale Geomechanics. ISTE/Wiley, pp. 86–112.
Barton, N., Kjaernsli, B., 1981. Shear strength of rockfills. J. Geotech. Eng. 107 (7), 873–891.
Blatz, J.A., Cui, Y.-J., Oldecop, L., 2008. Vapor equilibrium and osmotic technique for suction control. Geotech. Geol. Eng. 26 (6), 661–673.
Bozan, C., Wallis, I., Cook, P.G., Dogramaci, S., 2022. Groundwater-level recovery following closure of open-pit mines. Hydrogeol. J. 30, 1819–1832.
Brzesowsky, R.H., Hangx, S.J.T., Brantut, N., Spiers, C.J., 2014. Compaction creep of sands due to time-dependent grain failure: Effects of chemical environment, applied stress, and grain size. J. Geophys. Res. Solid Earth 119 (10), 7521–7541.
Chen, Q., Zhou, C.J., Wang, C., Zhou, C., 2021. Size effect on creep behavior and creep model of slate rockfill with oversized particles. Proc. Inst. Civil Eng.– Geotech. Eng. 176 (1), 3–14.
Decagon Devices, Inc, 2018. WP4C Water Dewpoint Potentiometer. Operator's Manual Version April 2018. Decagon Devices, Inc, Pullman, USA (www.decagon.com).
Duuring, P., Teitler, Y., Hagemann, S., 2017. Banded iron formation-hosted iron ore deposits of the Pilbara Craton. In: Phillips, G.N. (Ed.), Australian Ore Deposits. Australian Institute of Mining & Metallurgy (AusIMM), pp. 345–350.
Fredlund, D.G., Rahardjo, H., 1993. Soil Mechanics for Unsaturated Soils. John Wiley & Sons, Inc., New York, NY, USA.
Frossard, E., Hu, W., Dano, C., Hicher, P.-Y., 2012. Rockfill shear strength evaluation: a rational method based on size effects. Géotechnique 62 (5), 415–428.
Green, R., 2009. Holistic management of sulphides at Rio Tinto Iron Ore's Pilbara mine sites. Min. Technol. 118 (3–4), 232–237.
Hawley, P.M., Cunning, J., 2017. Guidelines for Mine Waste Dump and Stockpile Design. CSIRO Publishing.
Hoy, M., Doan, C.B., Horpibulsuk, S., Suddeepong, A., Udomchai, A., Buritatum, A., Chaiwan, A., Doncommul, P., Arulrajah, A., 2024. Investigation of a large-scale waste dump failure at the Mae Moh mine in Thailand. Eng. Geol. 329, 107400.
Hu, W., Dano, C., Hicher, P.-Y., Le Touzo, J.-Y., Derkx, F., Merliot, E., 2011. Effect of sample size on the behavior of granular materials. Geotech. Test. J. 34 (3), 186–197.
Indraratna, B., Wijewardena, L., Balasubramaniam, A., 1993. Large-scale triaxial testing of greywacke rockfill. Géotechnique 43 (1), 539–543.
Jacinto, A.C., Villar, M.V., Gomez-Espina, R., Ledesma, A., 2009. Adaptation of the van Genuchten expression to the effects of temperature and density for compacted bentonites. Appl. Clay Sci. 42 (3–4), 575–582.
Kepert, D., Clarke, N., Simpson, C., Edwards, D., 2010. Discovery of the Solomon iron deposits, Hamersley Province, Western Australia. Appl. Earth Sci. 119 (1), 21–27.
Lade, P., Karimpour, H., 2010. Static fatigue controls particle crushing and time effects in granular materials. Soil Found. 50 (5), 573–583.
Leussink, H., 1960. Bau eines grossen dreiaxialen shergerätes zur untersuchung grobkörniger erdstoffe (Design of a large triaxial shear apparatus for investigating coarse grained soils). In: Publication of the Soil Mechanics Institute of the Karlsruhe Technical University, Germany, Vol. 1.
Lim, W.L., McDowell, G.R., Collop, A.C., 2004. The application of Weibull statistics to the strength of railway ballast. Granul. Matter 6, 229–237.
Linero, S., Palma, C., Apablaza, R., 2007. Geotechnical characterization of waste material in very high dumps with large scale triaxial testing. In: Proceedings of International Symposium on Rock Slope Stability in Open Pit Mining and Civil Engineering, ed.: Potvin, Australian Centre for Geomechanics, Perth, Australia, pp. 59–75.
Linero, S., Fityus, S., Simmons, J., Cassidy, J., 2017. Trends in the evolution of particle morphology with size in colluvial deposits overlying channel iron deposits. Eur. Phys. J. Conf. 140, 14005.
Linero, S., Bradfield, L., Fityus, S., Simmons, J., Lizcano, A., 2020. Design of a 720 mm square direct shear box and investigation of the impact of boundary conditions on large scale measured strength. Geotech. Test. J. 43 (6), 1463–1480.
Mao, H., Shen, C., Liu, S., Wang, L., 2023. Insight into the crushing strength of rockfill grains at different temperature and relative humidity conditions. Rock Mech. Rock. Eng. 56, 6529–6543.
Marachi, N.D., Chan, C.K., Seed, H.B., Duncan, J.M., 1969. Strength and Deformation Characteristics of Rockfills Materials. Report no. TE-69-5, Department of Civil Engineering, University of California, Berkeley.
Marsal, R., 1967. Large-scale testing of rockfill materials. J. Soil Mech. Found. Div. ASCE 93 (SM2), 27–441.
McDowell, G.R., Bolton, M.D., 1998. On the micromechanics of crushable aggregates. Géotechnique 48 (5), 667–679.
Mesri, G., Godlewski, P.M., 1977. Time- and Stress-Compressibility Interrelationship. J. Geotech. Eng. Div. ASCE 103 (5), 417–430.
Mesri, G., Vardhanabhuti, B., 2009. Compression of granular materials. Can. Geotech. J. 46 (4), 369–392.
Morris, C., 1993. Genetic modelling for banded iron-formation of the Hamersley Group, Pilbara Craton, Western Australia. Precambrian Res. 60 (1–4), 243–286.
Nakata, Y., Hyde, A.F.L., Hyodo, M., Murata, H., 1999. A probabilistic approach to sand particle crushing in the triaxial test. Géotechnique 49, 567–583.
Oldecop, L., Alonso, E., 2001. A model for rockfill compressibility. Géotechnique 51 (2), 127–139.
Oldecop, L., Alonso, E., 2003. Suction effects on rockfill compressibility. Géotechnique 53 (2), 289–292.
Oldecop, L., Alonso, E., 2007. Theoretical investigation of the time dependent behavior of rockfill. Géotechnique 57 (3), 289–301.
Osses, R., Majdanishabestari, K., Ovalle, C., Pineda, J., 2021. Testing and modelling total suction effects on compressibility and creep of crushable granular material. Soils Found. 61 (6), 1581–1596.
Ovalle, C., 2018. Role of particle breakage in primary and secondary compression of wet and dry sand. Géotech. Lett. 8 (2), 161–164.
Ovalle, C., Hicher, P.-Y., 2020. Modeling the effect of wetting on the mechanical behavior of crushable granular materials. Geosci. Front. 11 (2), 487–494.
Ovalle, C., Frossard, E., Dano, C., Hu, W., Maiolino, S., Hicher, P.-Y., 2014. The effect of size on the strength of coarse rock aggregates and large rockfill samples through experimental data. Acta Mech. 225, 2199–2216.
Ovalle, C., Linero, S., Dano, C., Bard, E., Hicher, P.-Y., Osses, R., 2020. Data compilation from large drained compression triaxial tests on coarse crushable rockfill materials. J. Geotech. Geoenviron. Eng. 146 (9), 06020013.
Ovalle, C., Girumugisha, G., Cantor, D., Ouellet, S., 2023. Size effects assessment of mine waste-rock shear strength combining numerical, laboratory and in situ approaches. In: Dight, P.M. (Ed.), SSIM 2023: Third International Slope Stability in Mining Conference. Australian Centre for Geomechanics, Perth, pp. 291–300.
Scholz, C.H., 1968. Mechanism of creep in brittle rock. J. Geophys. Res. 73 (10), 3295–3302.
Sohn, C., Buscarnera, G., 2019. Measurement and simulation of comminution rate in granular materials subjected to creep tests. Granul. Matter 21 (60).
Steiakakis, E., Kavouridis, K., Monopolis, D., 2009. Large scale failure of the external waste dump at the "south Field" lignite mine, Northern Greece. Eng. Geol. 104, 269–279.
Ulusay, R., Arikan, F., Yoleri, M.F., Çağlan, D., 1995. Engineering geological characterization of coal mine waste material and an evaluation in the context of back-analysis of spoil pile instabilities in a strip mine, SW Turkey. Eng. Geol. 40 (1–2), 77–101.
Valenzuela, L., Bard, E., Campaña, J., Anabalón, M.E., 2008. 2008. High waste rock dumps — challenges and developments. In: Fourie, A.B. (Ed.), First International Seminar on the Management of Rock Dumps, Stockpiles and Heap Leach Pads. Australian Centre for Geomechanics, Perth, pp. 65–78.
Varadarajan, A., Sharma, K., Venkatachalam, K., Gupta, K., 2003. Testing and modeling two rockfill materials. J. Geotech. Geoenviron. Eng. 129 (3), 206–218.
Verdugo, R., De la Hoz, K., 2006. In: Ling, Hoe I., et al. (Eds.), Strength and Stiffness of Coarse Granular Soils. Soil Stress-Strain Behavior: Measurement, Modeling and Analysis. Springer, the Netherlands, pp. 243–252.
Wadell, H., 1932. Volume, shape, and roundness of rock particles. J. Geol. 40 (5), 443–451.
Weibull, W., 1939. A statistical theory of the strength of materials. In: Proceedings of Royal Swedish Institute of Engineering Research, p. 151.
Xu, M., Jina, D., Songa, E., Shenb, Z., Yangb, Z., Fub, F., 2019. Full-scale creep test and back-analysis of the long-term settlement of heavy loaded shallow foundations on a high rockfill embankment. Comput. Geotech. 115, 103156.
Yin, Z.-Y., Hicher, P.-Y., Dano, C., Jin, Y.-F., 2017. Modeling mechanical behavior of very coarse granular materials. J. Eng. Mech. 143 (1), C4016006.

Zapico, I., Molina, A., Laronne, J.B., Sánchez Castillo, L., Martín Duque, J.F., 2020. Stabilization by geomorphic reclamation of a rotational landslide in an abandoned mine next to the Alto Tajo Natural Park. Eng. Geol. 264, 105321.

Zhang, Y., Buscarnera, G., 2017. A rate-dependent breakage model based on the kinetics of crack growth at the grain scale. Géotechnique 67 (1), 953–967.

Zhou, X., Ma, G., Zhang, Y., 2019. Grain size and time effect on the deformation of rockfill dams: a case study on the Shuibuya CFRD. Géotechnique 69 (7), 606–619.